Monthly Notices
of the
ROYAL ASTRONOMICAL SOCIETY

MNRAS **467,** 985–995 (2017)
Advance Access publication 2017 January 20

doi:10.1093/mnras/stx170

The kinematic Sunyaev–Zel'dovich effect of the large-scale structure (I): dependence on neutrino mass

M. Roncarelli,[1,2]★ F. Villaescusa-Navarro[3,4,5] and M. Baldi[1,2,6]

[1]*Dipartimento di Fisica e Astronomia, Università di Bologna, viale Berti Pichat 6/2, I-40127 Bologna, Italy*
[2]*Istituto Nazionale di Astrofisica (INAF) – Osservatorio Astronomico di Bologna, via Ranzani 1, I-40127 Bologna, Italy*
[3]*Center for Computational Astrophysics, 160 Fifth Avenue, New York, NY 10010, USA*
[4]*Istituto Nazionale di Astrofisica (INAF) – Osservatorio Astronomico di Trieste, via Tiepolo 11, I-34131 Trieste, Italy*
[5]*Istituto Nazionale di Fisica Nucleare (INFN) – Sezione di Trieste, via Valerio 2, I-34127 Trieste, Italy*
[6]*Istituto Nazionale di Fisica Nucleare (INFN) – Sezione di Bologna, viale Berti Pichat 6/2, I-40127 Bologna, Italy*

Accepted 2017 January 18. Received 2017 January 17; in original form 2016 October 14

ABSTRACT

The study of neutrinos in astrophysics requires the combination of different observational probes. The temperature anisotropies of the cosmic microwave background induced via the kinematic Sunyaev–Zel'dovich (kSZ) effect may provide interesting information since they are expected to receive significant contribution from high-redshift plasma. We present a set of cosmological hydrodynamical simulations that include a treatment of the neutrino component considering four different sum of neutrino masses: $\Sigma m_\nu = (0, 0.15, 0.3, 0.6)$ eV. Using their outputs, we modelled the kSZ effect due to the large-scale structure after the reionization by producing mock maps, then computed the kSZ power spectrum and studied how it depends on $z_{\rm re}$ and Σm_ν. We also run a set of four simulations to study and correct possible systematics due to resolution, finite box size and astrophysics. With massless neutrinos we obtain $\mathcal{D}_{3000}^{\rm kSZ} = 4.0\ \mu{\rm K}^2$ ($z_{\rm re} = 8.8$), enough to account for all of the kSZ signal of $\mathcal{D}_{3000}^{\rm kSZ} = (2.9 \pm 1.3)\ \mu{\rm K}^2$ measured with the South Pole Telescope. This translates into an upper limit on the kSZ effect due to patchy reionization of $\mathcal{D}_{3000}^{\rm kSZ,patchy} < 1.0\ \mu{\rm K}^2$ (95 per cent confidence level). Massive neutrinos induce a damping of kSZ effect power of about 8, 12 and 40 per cent for $\Sigma m_\nu = (0.15, 0.3, 0.6)$ eV, respectively. We study the dependence of the kSZ signal with $z_{\rm re}$ and the neutrino mass fraction, f_ν, and obtain $\mathcal{D}_{3000}^{\rm kSZ} \propto {z_{\rm re}}^{0.26}(1 - f_\nu)^{14.3}$. Interestingly, the scaling with f_ν is significantly shallower with respect to the equivalent thermal SZ effect, and may be used to break the degeneracy with other cosmological parameters.

Key words: neutrinos – methods: numerical – cosmic background radiation – cosmology: theory – large-scale structure of Universe.

1 INTRODUCTION

In the last decade, the study of the neutrinos properties has seen an increasing interest in both the fields of particle physics and astrophysics. While the particle physics Standard Model (SM) considers the existence of three active massless neutrino species, namely the electron, mu and tau neutrinos, the detection of leptonic flavour oscillation of solar and atmospheric neutrinos (Fukuda et al. 1998; Ahmad et al. 2001, 2002) indicates that these particles have a non-zero mass. The following studies in this field allowed to fix a lower limit on the sum of the three neutrino masses of $\Sigma m_\nu > 0.06$ eV[1] (95 per cent confidence level (CL), see Lesgourgues & Pastor 2006, 2012, 2014; Lesgourgues et al. 2013; Gonzalez-Garcia 2014, and references therein).

From the astrophysical point of view, the existence of massive neutrinos influences the evolution of the large-scale structure (LSS) formation via gravitational interaction, thus requiring a generalization of the standard Λ cold dark matter (ΛCDM) cosmological model to account for Σm_ν as an additional free parameter, leading to a ΛCDMν scenario. The effect of this new component is twofold. On early times it contributes to the Universe energy budget as radiation, with density of

$$\rho_\nu = \frac{7}{8}\left(\frac{4}{11}\right)^{\frac{4}{3}} N_{\rm eff}\,\rho_\gamma, \tag{1}$$

where ρ_γ is the photon energy density and $N_{\rm eff}$ is the effective number of neutrino species ($N_{\rm eff} = 3.046$, according to the SM). This causes a postponing of the matter–radiation equality for a

★ E-mail: mauro.roncarelli@unibo.it

[1] This limit applies in the case of normal hierarchy, for the inverted hierarchy, the limit is $\Sigma m_\nu > 0.1$ eV.

fixed value of $\Omega_{\rm m}\,h^2$ (where $\Omega_{\rm m}$ is the ratio between the total matter density of the Universe and the critical one, $\rho_{\rm c}$, at the present epoch and h is the Hubble constant H_0 in units of $100\,{\rm km\,s^{-1}\ Mpc^{-1}}$). At late times, the neutrinos' large thermal velocities prevent their clustering on scales smaller than their free-streaming length

$$\lambda_{{\rm fs},\nu} \simeq 7.67\,\frac{H_0(1+z)^2}{H(z)}\left(\frac{1\,{\rm eV}}{m_\nu}\right)h^{-1}\,{\rm Mpc}. \qquad (2)$$

This induces a gravitational backreaction that suppresses density fluctuations of both baryons and CDM on the same scales. Thus, as a net effect, massive neutrinos cause a suppression in the amplitude of the matter power spectrum on small scales with respect to an equivalent massless neutrinos model.

The dependence of these effects on the total neutrino mass indicates that astrophysical observations have the potential to provide constraints on the value of Σm_ν, as it has been shown by several recent theoretical works (see e.g. Viel, Haehnelt & Springel 2010; Marulli et al. 2011; Shimon et al. 2012; Carbone 2013; Costanzi Alunno Cerbolini et al. 2013; Mak & Pierpaoli 2013; Palanque-Delabrouille et al. 2015; Roncarelli, Carbone & Moscardini 2015). In fact, the list of cosmological probes that can be used to place limits on the sum of neutrino masses is nowadays long and heterogeneous, including galaxy redshift surveys (Elgarøy et al. 2002; Tegmark et al. 2006; Thomas, Abdalla & Lahav 2010), galaxy clustering (Saito, Takada & Taruya 2011; Zhao et al. 2013; Beutler et al. 2014; Sánchez et al. 2014), cosmic microwave background (CMB) observations from the *Wilkinson Microwave Anisotropy Probe* (*WMAP*; Komatsu et al. 2009, 2011; Hinshaw et al. 2013) and *Planck* (Planck Collaboration XIII 2016), Ly-α forest studies (Croft, Hu & Davé 1999; Viel et al. 2010; Palanque-Delabrouille et al. 2015), galaxy clusters mass function (Mantz, Allen & Rapetti 2010; Mantz et al. 2015) and future 21cm intensity mapping observations (Villaescusa-Navarro, Bull & Viel 2015).

Most notably, the current tightest constraints on the sum of the neutrino masses have been derived by Palanque-Delabrouille et al. (2015) who combined data from the CMB with BAO and Ly-α forest and obtained an upper limit (95 per cent CL) of $\Sigma m_\nu \leq 0.14\,{\rm eV}$ (see also Cuesta, Niro & Verde 2016, for a different analysis combing CMB and galaxy clustering). It should be noted, however, that all these bounds have been derived assuming that massive neutrinos evolve in an otherwise standard ΛCDM cosmological model. Possible alternative scenarios such as non-standard dark energy or modified gravity theories may result in significantly looser constraints (see e.g. La Vacca et al. 2009; He 2013; Motohashi, Starobinsky & Yokoyama 2013; Baldi et al. 2014). Furthermore, the first release of *Planck* satellite data highlighted a discrepancy between the cosmological parameters obtained with primary CMB observations (Planck Collaboration XVI 2014) and the relatively low number counts of galaxy clusters detected via thermal Sunyaev–Zel'dovich (tSZ; Sunyaev & Zeldovich 1970) effect: the joint analysis of these data sets and BAO data led to an estimate of $\Sigma m_\nu = (0.20 \pm 0.09)\,{\rm eV}$ (Planck Collaboration XX 2014). However, this result is hampered by the degeneracy with the other cosmological parameters (mainly σ_8 and $\Omega_{\rm m}$) and by the uncertainty in the amount of non-thermal pressure contribution in galaxy clusters. Indeed, more recently the analysis of the latest *Planck* data release (Planck Collaboration XXIV 2016) showed that the attempt to reconcile primary CMB and cluster counts by increasing Σm_ν only leads to a conflict with H_0 measurements from BAO (see also the discussion in Leistedt, Peiris & Verde 2014; Planck Collaboration XIII 2016). This indicates that the origin of this tension is not fully understood and that additional efforts involving other observational probes are necessary.

In this framework, new potentially interesting observational constraints may come from the kinematic Sunyaev-Zel'dovich (kSZ) effect, i.e. a secondary anisotropy of the CMB caused by the motion of free electrons of the LSS, whose dependence on the physical properties of the intergalactic medium (IGM) is complementary in many aspects with respect to the tSZ one (see e.g. Roncarelli et al. 2007; Battaglia et al. 2010; Shaw, Rudd & Nagai 2012). In particular, the kSZ effect is expected to be sensitive to the IGM residing in non-collapsed structures at high redshift. While several new generation microwave telescopes have reached the sensitivity to achieve the first kSZ effect detections on galaxy clusters (Hand et al. 2012; Sayers et al. 2013; Planck Collaboration XXXVII 2016), up to now the only measurement of its power spectrum has been obtained with the South Pole Telescope (SPT) by Crawford et al. (2014) and by George et al. (2015). By combining the tSZ bispectrum from the SPT-SZ survey (800 deg^2) with the full 2540 deg^2 field, they measured an amplitude of the kSZ temperature fluctuations of $\mathcal{D}^{\rm kSZ}_{3000} = (2.9 \pm 1.3)\,\mu{\rm K}^2$ at $\ell = 3000$. This places the first interesting constraint on a quantity that is expected to receive contribution from the LSS of the ionized Universe and from the epoch of reionization (EoR) itself. While the latter is extremely uncertain and depends on subtle details of the reionization process (see Iliev et al. 2014, and references therein), the kSZ effect of the post-ionization era can be studied with suitable LSS simulations and depends mostly on the cosmological assumptions. This gives the kSZ effect, the potential to provide constraints on several cosmological parameters, including Σm_ν.

This paper is the first of a series of studies of the kSZ effect from the LSS of the Universe in different cosmological scenarios beyond the standard ΛCDM paradigm. In this work, we present the first analysis of the kSZ effect derived from a set of cosmological hydrodynamical simulations that include a detailed treatment of the massive neutrino component (Viel et al. 2010). Our simulations follow the evolution of structure formation from large scales ($L_{\rm box} = 240\,h^{-1}$ Mpc) down to the non-linear regime spanning all the relevant redshifts. By analysing the outputs of the baryonic component, adopting a minimum number of assumptions, we derive a set of Doppler b-parameter maps and compute the corresponding power spectrum of kSZ-induced CMB temperature fluctuations in the multipole range of $1000 < \ell < 20\,000$. This allows us to make a direct comparison with the SPT measurement and to derive how our results depend on the value of the redshift of reionization, $z_{\rm re}$, and Σm_ν.

This paper is organized as follows. In the next section, we describe the simulation set used in this work, our procedure to create mock light-cones and our kSZ effect model. In Section 3, we present our results in terms of the effect of neutrino mass on the global properties of the kSZ effect and discuss the dependence with $z_{\rm re}$. Section 4 is devoted to the study of possible systematics caused by limited box size, finite resolution and accuracy of the astrophysical processes of our simulations. We summarize and draw our conclusions in Section 5.

2 MODELLING THE EFFECT OF NEUTRINOS ON THE kSZ SIGNAL

2.1 The simulation set

We have run hydrodynamical simulations using the TREEPM+smoothed particle hydrodynamics (SPH) code GADGET-III

Table 1. Parameter values of our simulation suite. First column: simulation name. Second column: comoving box size, in h^{-1} Mpc. Third column: total number of particles, including all three species (two in case of massless neutrinos). Fourth to sixth column: masses of the CDM, baryonic and neutrino particles, respectively, in units of $10^9\,h^{-1}\,\mathrm{M}_\odot$. Seventh to ninth column: sum of neutrino masses, Σm_ν, in eV, corresponding value of neutrino mass fraction, $f_\nu = \Omega_\nu/\Omega_\mathrm{m}$, in percent units, and σ_8 at present epoch, respectively. The last column shows the physical model(s) assumed for the baryonic component (radiative cooling and UV background are present in all simulations, see text for details). All simulations assume a flat ΛCDM(ν) cosmology with $\Omega_\Lambda = 0.6825$, $\Omega_\mathrm{m} = \Omega_\mathrm{CDM} + \Omega_\mathrm{b} + \Omega_\nu = 0.3175$, $H_0 = 67.11\,\mathrm{km\,s^{-1}\,Mpc^{-1}}$ ($h = 0.6711$), $n_s = 0.9624$ and $A_s = 2.13 \times 10^{-9}$.

Simulation	L_box (h^{-1} Mpc)	N_p	$m_\mathrm{p,cdm}$	$m_\mathrm{p,b}$ ($10^9\,h^{-1}\,\mathrm{M}_\odot$)	$m_\mathrm{p,\nu}$	Σm_ν (eV)	$10^2 f_\nu$	σ_8 ($z = 0$)	Baryon physics (+ rad. cooling + UV bkg.)
N0	240	2×512^3	7.68	1.40	–	0	0	0.834	quick Ly-α
N15	240	3×512^3	7.57	1.40	0.10	0.15	1.11	0.801	quick Ly-α
N30	240	3×512^3	7.47	1.40	0.20	0.30	2.23	0.764	quick Ly-α
N60	240	3×512^3	7.27	1.40	0.40	0.60	4.46	0.693	quick Ly-α
HR	240	2×1024^3	0.96	0.18	–	0	0	0.834	quick Ly-α
SB	120	2×256^3	7.68	1.40	–	0	0	0.834	quick Ly-α
LB	480	2×1024^3	7.68	1.40	–	0	0	0.834	quick Ly-α
CSFW	240	2×512^3	7.68	1.40	–	0	0	0.834	star form. + SN feedback

(Springel 2005) for four different cosmologies with massless and massive neutrinos. The value of the following cosmological parameters are common to all models: Ω_m=$\Omega_\mathrm{CDM} + \Omega_\mathrm{b} + \Omega_\nu = 0.3175$, $\Omega_\mathrm{b} = 0.049$, $\Omega_\Lambda = 0.6825$, $h = 0.6711$, $n_s = 0.9624$, $A_s = 2.13 \times 10^{-9}$ (corresponding to $\sigma_8 = 0.834$ at $z = 0$ in the ΛCDM scenario), in agreement with the latest results by Planck Collaboration XIII (2016). In models with massive neutrinos, we set $\Omega_\nu h^2 = \Sigma m_\nu$ /(93.14eV) and modified the value of Ω_CDM accordingly to keep Ω_m constant. In our fiducial runs, we follow the evolution of 512^3 CDM plus 512^3 gas plus 512^3 neutrino particles (only in models with massive neutrinos). A summary of the simulation parameters is shown in Table 1.

The initial conditions of the simulations have been generated by placing each particle species (CDM, gas and neutrinos) in a different regular cubic grid, then displacing and assigning them peculiar velocities using the Zel'dovich approximation. To this purpose, we rescaled the matter $z = 0$ power spectra and transfer functions, computed with CAMB (Lewis, Challinor & Lasenby 2000), to the starting redshift of the simulations that we fix to $z = 99$. This rescaling was done using the Newtonian physics implemented in the numerical simulation. For cosmologies with massive neutrinos, this is translated into a scale dependence growth factor and rate in both the CDM and neutrino power spectra.[2] For further details, we refer the reader to Zennaro et al. (2016). We also assigned thermal velocities, besides peculiar ones, to neutrino particles by randomly sampling the neutrino Fermi–Dirac momentum distribution.

In our first simulation set, dubbed N0, N15, N30 and N60 in Table 1, we fixed the comoving box size to $L_\mathrm{box} = 240\,h^{-1}$ Mpc and varied only the neutrino mass assuming four different values: $\Sigma m_\nu = (0, 0.15, 0.3, 0.6)$ eV, respectively. All other parameters have been kept identical, including the random seeds of the initial conditions, ensuring that we actually model the evolution of the same structures down to $z = 0$. In order to study systematic effects (see Section 4), we have run a second set of four simulations assuming massless neutrinos. The first one, dubbed HR, has higher resolution (2×1024^3 particles) and same box size. The following two, SB and LB, have different comoving box sizes, (120, 480) h^{-1} Mpc, respectively, to investigate the dependence of our results on the simulation volume: in order to keep the same mass resolution, we used 2×256^3 and 2×1024^3 particles for the SB and LB runs, respectively. Finally, a last simulation, dubbed CSFW, assumes same resolution and box size of the N0 but adopts a different physical treatment for the baryonic component, allowing us to study the dependence of our results with the astrophysical processes that affect the IGM. For each simulation, we have produced a set of 26 snapshots at different redshifts from $z = 15$ down to the present epoch. This ensures that we can reconstruct the full line of sight of the kSZ signal.

All our hydrodynamical simulations include radiative cooling by hydrogen and helium and heating by a uniform UV background. The cooling routine has been modified in order to reproduce the measured Universe thermal history as in Viel et al. (2013). In order to save computational time, we have run our simulations (except the CSFW simulation) using the so-called 'quick Ly-α' technique. This method consists in following the hydrodynamical evolution of the gas particles until their densities reach a given threshold, beyond which the code turns them into star particles and turns off the hydrodynamic forces. In order to verify that our results are not largely affected by this simplistic physics model, in our CSFW run, we implemented star formation and supernova (SN) feedback following Springel & Hernquist (2003), instead of the quick Ly-α method. SN feedback is implemented as kinetic feedback, with constant velocity winds of $350\,\mathrm{km\,s^{-1}}$.

While the modelling of the X-ray emission and of the tSZ effect depends highly on the assumptions on cooling and feedback, the global kSZ signal due to the LSS after the reionization shows a much weaker dependence on the physical scheme adopted for the baryonic component,[3] with the only meaningful uncertainty that resides in the amount of cosmic gas that is not in the ionized state (see e.g. Roncarelli et al. 2007; Trac, Bode & Ostriker 2011; Shaw, Rudd & Nagai 2012). Given the negligible amount of mass associated with neutral and molecular hydrogen, this translates into determining the correct stellar mass fraction as a function of redshift. It is well known that the quick Ly-α cooling scheme cannot reproduce a realistic star formation history, as it can be seen in the plot of Fig. 1 that shows the stellar mass fraction, $f_\star \equiv \rho_\star/\rho_\mathrm{b}$, as a function of redshift obtained from the raw output of our simulations. As expected, the main difference is due to the change in the gas particle resolution,

[2] The rescaling is performed using the REPS code: https://github.com/matteozennaro/reps

[3] This, of course, is not true for the possible patchy kSZ effect imprinted during the EoR, which would add to the one subject of our study.

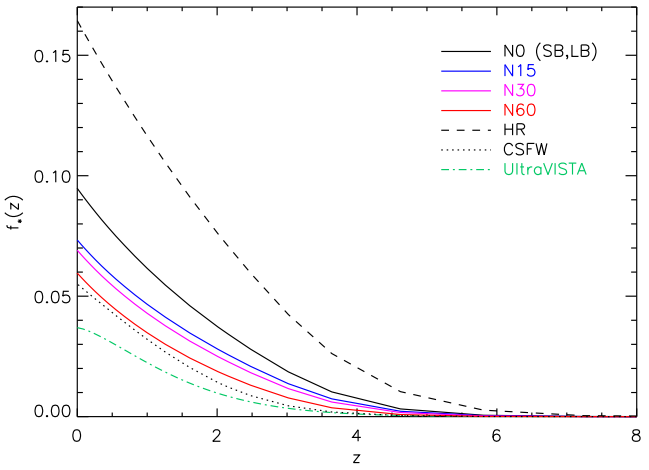

Figure 1. Global star mass fraction ($\rho_\star/\rho_b$) in the whole box volume as a function of redshift for the eight simulations. Solid lines indicate our first simulation set with $\Sigma m_\nu = (0, 0.15, 0.3, 0.6)$ eV shown in black, blue, magenta and red, respectively. The black dashed and dotted lines correspond to the HR and CSFW simulations, respectively. The values of $f_\star(z)$ for the SB and LB simulations (not shown) are very close to the N0 ones (see details in Table 1). The green dot–dashed line is derived from the cosmic stellar mass density estimated by Ilbert et al. (2013).

with higher resolution predicting higher star formation, and with neutrino mass changes that produce smaller effects. We compare these results to the ones obtained with the UltraVISTA data by Ilbert et al. (2013, green dot–dashed line): we observe that in all cases, our models predict a significant excess of star formation, with our N0 model that ends at $z = 0$ with $f_\star \simeq 9.5$ per cent compared to the observed $f_\star \simeq 3.8$ per cent. The CSFW model, thanks to its feedback scheme, shows more realistic values of $f_\star$ but still in excess with respect to the observed ones. To overcome this issue, for the purpose of this work we assume the $f_\star(z)$ value by Ilbert et al. (2013) and apply a correction a posteriori to the differential kSZ signal at all redshifts to account for this difference. We will discuss this point in detail in Section 2.3.

2.2 Light-cone construction

In order to model the kSZ effect integrated along the line of sight, we need to use the outputs of our simulations to reconstruct the full light-cone geometry from $z = 0$ up to the EoR. Our method is similar to the one adopted in our previous papers (see e.g. Roncarelli et al. 2010, 2012, 2015): we refer the reader to these works for the details, and we just summarize here the main points.

We stack the different simulation volumes along the line of sight up to $z = 15$, corresponding to $7022\,h^{-1}$ comoving Mpc. To avoid the repetition of the same structures along the line of sight, we randomize every simulation volume in the following ways: (i) we assign to each Cartesian axis a 50 per cent probability to be reflected; (ii) we randomly pick the axis oriented along the line of sight and the two perpendicular ones; (iii) we recenter randomly the coordinates by using the periodic boundary conditions; (iv) and for distances that assure that the box volume does not exceed the opening angle of the light-cone, the cube is rotated by a random angle around the line of sight passing through its centre. This process is done using the same random seeds for all simulations: since we are also using the same phases in the initial conditions, this ensures that we represent exactly an identical realization of the comoving volume[4] with different models, eliminating the effect of cosmic variance when comparing them. To increase the statistical accuracy of our results, we generate 50 different light-cone realizations by varying the seed of the full randomization process.

In order to optimize the redshift sampling, each simulation volume is divided along the line of sight into slices associated with different simulation outputs: their limits are defined in a way that ensures that for every comoving distance, we chose the snapshot that better matches the corresponding age of the Universe in our cosmological model.

The maximum opening angle of the light-cone is limited by the angular box size at $z = 15$: this allows us to fix it to $1.^\circ8$ for all simulations, except the SB for which we are limited to $0.^\circ9$. When accounting for the 50 light-cone realizations this corresponds to a total sky area of 162 deg^2 (40.5 deg^2 for the SB). We point out that this area can be considered fully independent only up to $z \sim 0.4$ because at higher redshifts, the light-cones geometry starts to replicate to some extent the same structures in the different realizations, and includes almost all the simulation volume at $z = 15$. However, this issue is compensated by the decrease of cosmic variance at high redshift.

2.3 The kSZ effect model

The kSZ effect (also referred to as the Ostriker–Vishniac effect in the linear-theory approximation; Ostriker & Vishniac 1986; Vishniac 1987) is the Doppler shift of the CMB photons caused by the interaction with free electrons of the IGM that have a proper motion with respect to the CMB rest frame. Its intensity in a given direction with unit vector $\hat{\gamma}$ can be expressed using the Doppler b-parameter, defined as

$$b(\hat{\boldsymbol{\gamma}}) \equiv \frac{\sigma_\mathrm{T}}{c} \int_0^{z_\mathrm{re}} \frac{\mathrm{d}\chi}{\mathrm{d}z} \frac{\mathrm{d}z}{1+z} \, \mathrm{e}^{-\tau(z)} \, n_\mathrm{e} \, \boldsymbol{v}_\mathrm{e} \cdot \hat{\boldsymbol{\gamma}} \,, \tag{3}$$

where σ_T is the Thomson cross-section, c is the light speed in vacuum, n_e is the electron number density and $\boldsymbol{v}_\mathrm{e}$ is the proper velocity of the electrons. The integral is calculated from the observer up to z_re along the comoving coordinate χ. In the previous equation, τ is the Thomson optical depth:

$$\tau(z) \equiv \sigma_\mathrm{T} \int_0^z \frac{\mathrm{d}\chi}{\mathrm{d}z'} \frac{\mathrm{d}z'}{1+z'} \, n_\mathrm{e}(z') \,. \tag{4}$$

Once the value of b is known, the corresponding change in the observed CMB temperature measurement is simply

$$\Delta T = -b \, T_\mathrm{CMB} \,, \tag{5}$$

thus independent of observational frequency, with approaching (receding) gas that induces a temperature increment (decrement).

While it is known that possible non-uniform reionization scenarios can imprint a non-negligible kSZ effect associated with the EoR (see e.g. McQuinn et al. 2005; Zahn et al. 2005; Iliev et al. 2007, 2008; Mesinger, McQuinn & Spergel 2012, and references therein), this would require simulations that include a detailed modelling of both reionization sources and radiative transfer, and is therefore beyond the scope of this paper. Since we focus only on the kSZ of the LSS after the EoR, we can safely assume that the

[4] This does not apply completely for the SB and LB simulations, whose comoving box has a different size.

Universe is fully ionized, leaving $z_{\rm re}$ as a free parameter, and apply instead the following equation:

$$b(\hat{\boldsymbol{\gamma}}) = \frac{\sigma_{\rm T} X x_{\rm e}}{c\, m_{\rm p}} \int_0^{z_{\rm re}} \frac{{\rm d}\chi}{{\rm d}z} \frac{{\rm d}z}{1+z}\, {\rm e}^{-\tau(z)}\, \rho_{\rm g}\, \boldsymbol{v}_{\rm g} \cdot \hat{\boldsymbol{\gamma}}\,, \tag{6}$$

being $X = 0.76$ the cosmological hydrogen mass fraction, $x_{\rm e} \simeq 1.16$ the electron-to-proton ratio in a fully ionized primordial plasma, $m_{\rm p}$ the proton mass and $\rho_{\rm g}$ the gas mass density.

As said in Section 2.1, with this approach the main uncertainty resides in an accurate modelling of the star mass fraction, since one can safely assume that $\rho_{\rm g} = \rho_{\rm b}(1 - f_\star)$. The output of our hydrodynamical simulations already provides the value of the cosmological gas density, however, given the bias shown in Fig. 1, we correct the output in the following way:

$$\rho_{\rm g}(z) = \rho_{\rm g,sim}(z) \left[\frac{1 - f_{\star,\rm obs}(z)}{1 - f_{\star,\rm sim}(z)}\right]\,, \tag{7}$$

where $f_{\star,\rm sim}(z)$ and $f_{\star,\rm obs}(z)$ are the star mass fractions from the simulation and from Ilbert et al. (2013) results, respectively, as a function of redshift. This correction is applied globally to all the signal coming from the same redshift slice (see Section 2.2), thus neglecting the actual spatial distribution of star particles. However, this modification produces only minor differences in our final results (see the discussion in Section 4).

2.4 The mapping procedure

We used our simulations to create a set of b-parameter maps from which we derive our results on the kSZ effect. The mapping procedure is coherent with the SPH formalism and is described in detail in our previous works (see Roncarelli et al. 2006, 2007, 2012; Ursino, Galeazzi & Roncarelli 2010). We summarize here the main points.

For every SPH particle that falls inside the light-cone, we consider the output physical quantities that determine the kSZ effect, namely its mass, m_i, radial velocity, $v_{r,i} \equiv \boldsymbol{v}_i \cdot \hat{\boldsymbol{\gamma}}$, and angular diameter distance from the observer, $d_{{\rm A},i}$. We also include particles whose centre falls outside the light-cone but whose sphere with radius given by its SPH smoothing length, h_i, intersects its border. We then determine the integrated b-parameter of each SPH particle as

$$B_i = \frac{X\, \sigma_{\rm T}\, x_{\rm e}}{m_{\rm p}\, c\, d_{{\rm A},i}^2}\, e^{-\tau(z_i)}\, m_i\, v_{r,i}\,, \tag{8}$$

where z_i is the cosmological redshift in the particle's position. Finally, the values of B_i are used to convert the line-of-sight integral of equation (6) into a sum over the SPH particles and distributed over the map pixels close to the particle's centre, by adopting the same smoothing kernel used by the hydrodynamical code.

For the purpose of our work, we create maps of 1024 pixels per side. Given the map size of $1\overset{\circ}{.}8$ per side ($0\overset{\circ}{.}9$ for the SB simulation), this corresponds to an angular resolution of 6.33 arcsec (3.16 arcsec). This procedure is repeated for all the simulations and for the 50 light-cones. In addition, to study the redshift dependence of our results and to account for the uncertainty in the value of $z_{\rm re}$, we compute the integral separately for 20 logarithmically equispaced redshift bins. This makes a total of 1000 b-parameter maps for each simulation.

3 RESULTS

3.1 Global properties of the Doppler b-parameter

We show in Fig. 2 the b-parameter maps obtained with our method for different values of Σm_ν (first simulation set) for the same light-cone realization. For these maps, we assumed as integration limit (see equations 3 and 6) the nominal value of $z_{\rm re} = 8.8$ from Planck Collaboration XIII (2016). The typical values are of the order of $|b| \approx 10^{-6}$, with peaks that reach 10^{-5} associated with galaxy clusters and groups. However, the main coherent structures that can be seen in these maps are at larger angular scales, about 10 arcmin, and are associated with the bulk motions of the LSS. As expected, the presence of massive neutrinos slows down the growth of structure formation, damping velocity amplitudes at all redshifts. The consequence is that for increasing neutrino mass the amplitude of the kSZ effect is significantly reduced, both for peaks and for typical values: this can be seen by comparing qualitatively the four maps, where the same structures are present, with lower intensities for increasing Σm_ν.

This effect is shown in detail in Fig. 3, where we plot the probability distribution functions of the map pixels, computed considering the full set of 50 light-cones. All distributions peak around zero as expected by definition, but the dispersion decreases for higher values of Σm_ν. We find that all curves can be fit by a Gaussian distribution with mean and dispersion left as a free parameter. The results of the fit for the dispersion are quoted in the same plot, with σ_b going from 1.34×10^{-6} for massless neutrinos (in agreement with Roncarelli et al. 2007) to 1.05×10^{-6} in the case of $\Sigma m_\nu = 0.6$ eV. Following Roncarelli et al. (2015), we study its dependence on f_ν. We find that the relation between the two quantities can be fitted with a power-law function, and obtain that σ_b scales as

$$\sigma_{b,\nu} = \sigma_{b,0}\,(1 - f_\nu)^{5.2}\,, \tag{9}$$

being $\sigma_{b,0}$ the value for the ΛCDM model.

3.2 The kSZ effect power spectrum

One of the most important observables for the kSZ effect is its angular power spectrum, whose specific features can allow to break the degeneracy with other sources of CMB anisotropies (see e.g. Crawford et al. 2014). Using our set of b-parameter maps, we first convert them into ΔT using equation (5), then apply the Fast Fourier Transform method in the flat-sky approximation to compute the amplitude of the angular power spectrum of the kSZ temperature fluctuations as a function of the multipole ℓ. We report the results in terms of $\mathcal{D}_\ell$, defined as

$$\mathcal{D}_\ell \equiv \frac{\ell(\ell+1)\, C_\ell}{2\pi}\,, \tag{10}$$

being C_ℓ the usual definition of power spectrum of temperature fluctuations. We show in Fig. 4 the power spectra of our first simulation set obtained as the average over the 50 light-cones. In all cases, the amplitude, $\mathcal{D}_\ell^{\rm kSZ}$, of the kSZ power spectrum increases from $\ell = 1000$ to 6000, with a flattening for higher multipoles: this is consistent with what was found in previous works (Roncarelli et al. 2007; Trac et al. 2011; Shaw et al. 2012). The cosmic variance in the map fields for the N0 simulation (grey-shaded area) decreases with increasing multipole, from about 1 $\mu{\rm K}^2$ at $\ell = 1000$ to 0.5 $\mu{\rm K}^2$ at $\ell = 20\,000$. Interestingly, our N0 model shows a value of $\mathcal{D}_{3000}^{\rm kSZ} = 3.21\ \mu{\rm K}^2$, enough to explain all of the SPT measurement of $\mathcal{D}_{3000}^{\rm kSZ} = (2.9 \pm 1.3)\ \mu{\rm K}^2$ measured by George et al. (2015). Since our method is expected to underestimate the true

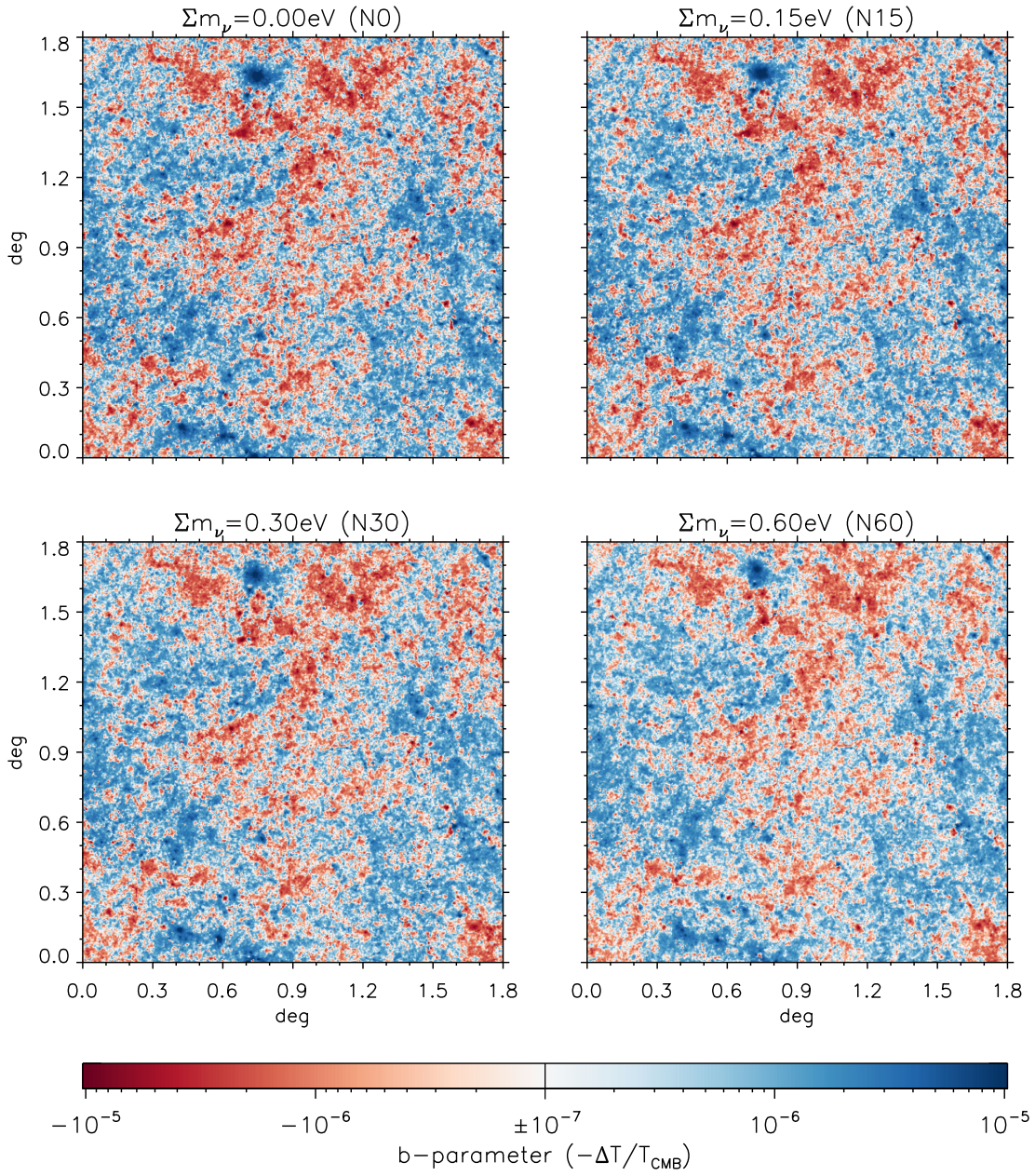

Figure 2. Maps of the b-parameter as a function of Σm_ν. Each map is $1\overset{\circ}{.}8$ per side with a resolution of 6.33 arcsec (1024^2 pixels) and represents the signal integrated from $z = 0$ to $z_{\rm re} = 8.8$ for the same light-cone assuming massless neutrinos (top left-hand panel) and $\Sigma m_\nu = (0.15, 0.3, 0.6)$ eV (top right-hand, bottom left-hand and bottom right-hand panels, respectively). The colour scale indicates in red the sky regions where, on average, the gas is approaching the observer ($b < 0$ and increase of observed CMB temperature), and in blue where the gas is receding ($b > 0$ and decrease of observed CMB temperature).

value by about 20 per cent due to the limited box size (see Section 4 for the details), this significantly reduces the amount of signal left that may be due to patchy reionization in a ΛCDM cosmology consistent with the results of Planck Collaboration XIII (2016), as we will discuss in Section 4.

Massive neutrinos induce a suppression of the amplitude of the kSZ power spectrum at all multipoles, slightly more pronounced at small scales. In our most extreme model, N60, the power is reduced by 40 per cent at $\ell = 1000$ and by half at $\ell > 10\,000$. However, when assuming more realistic scenarios given by the N15 and N30 simulations, the decrease of power at the same scales is significantly smaller, 8 and 12 per cent, respectively. These differences can be compared with the kSZ measurement by George et al. (2015, green diamond): all four models fall inside the 1σ interval, indicating that such difference would be difficult to measure with current instruments. Nonetheless we point out that if a significant additional kSZ effect associated with the EoR is present (see e.g. the relatively high values predicted by Iliev et al. 2008 and Mesinger et al. 2012), then the presence of massive neutrinos would help to alleviate the tension between observations and theory.

It is known that the amplitude and shape of the kSZ power spectrum depends on many cosmological parameters (see e.g. Shaw et al. 2012). With our method, we can easily study the dependence on $z_{\rm re}$ by varying the integration limit of our light-cones. We show in Fig. 5 how the amplitude, $\mathcal{D}^{\rm kSZ}_{3000}$, of the kSZ power spectrum at $\ell = 3000$ increases as a function of redshift. It is important to note

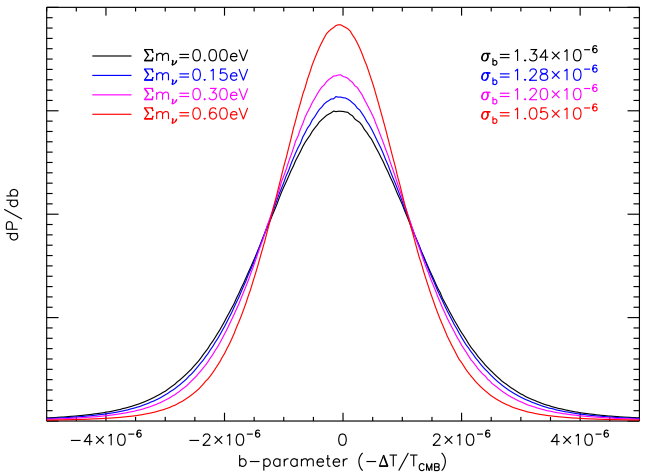

Figure 3. Probability distribution function of the b-parameter for different neutrino masses. Each curve is computed for the whole set of 50 light cones (i.e. 50 sets of maps like the ones shown in Fig. 2) with signal integrated up to $z_{\rm re} = 8.8$ and pixels of 6.33 arcsec per side. The black line indicates the model with massless neutrinos while $\Sigma m_\nu = (0.15, 0.3, 0.6)$ eV are shown in blue, magenta and red, respectively. On the right hand side, we show the standard deviation of the best-fitting Gaussian distribution of each curve.

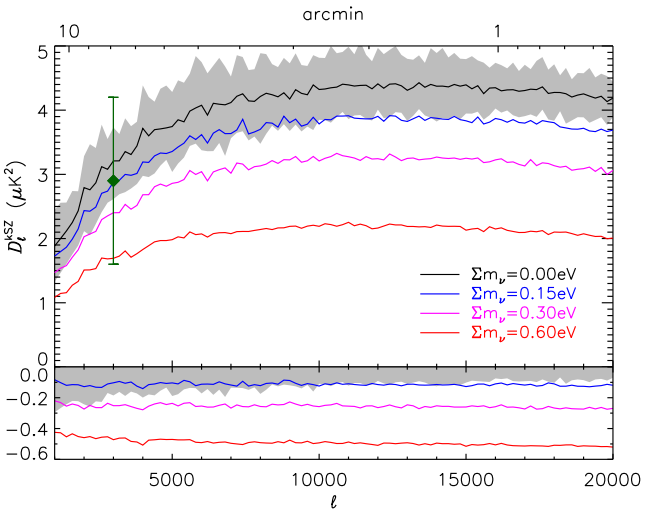

Figure 4. Top panel: angular power spectrum of temperature fluctuations associated with the kSZ effect ($\mathcal{D}_\ell^{\rm kSZ}$) as a function of the multipole ℓ for different values of Σm_ν. The curves are computed by averaging over the full set of 50 light-cones (a total of 162 deg^2) and consider the signal integrated up to $z_{\rm re} = 8.8$. The colour coding of the lines is the same as in Fig. 3. The grey-shaded area encloses the central 34 light-cones (68 per cent of the total) for the N0 model only. The green diamond with error bars shows the measurement of $\mathcal{D}_{3000}^{\rm kSZ} = (2.9 \pm 1.3)$ μK^2 by George et al. (2015). Bottom panel: relative differences with respect to the N0 model.

how the kSZ effect receives a significant contribution from both low and very high redshift gas: again, this is in agreement with previous findings (Roncarelli et al. 2007; Shaw et al. 2012). More precisely, for the N0 model if we assume $z_{\rm re} = 8.8$ (15), then 61 (52) per cent of the value of $\mathcal{D}_{3000}^{\rm kSZ}$ is due to gas located at $z < 2$. When introducing massive neutrinos the decrease of the kSZ signal shows no significant differences with redshift, even if the damping is slightly more prominent at low redshift where non-linear structure formation becomes important. For $\Sigma m_\nu = (0.15, 0.3, 0.6)$ eV and in the range $6 < z_{\rm re} < 15$, the value of $\mathcal{D}_\ell^{\rm kSZ}$ is smaller by about 10, 15 and

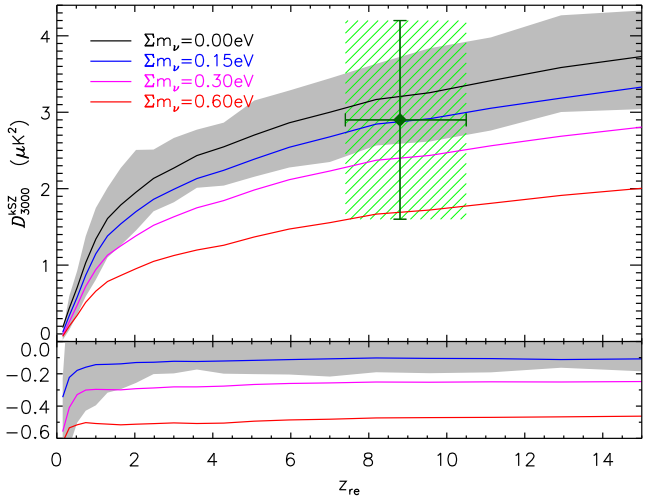

Figure 5. Top panel: amplitude of the kSZ power spectrum at $\ell = 3000$ ($\mathcal{D}_{3000}^{\rm kSZ}$) as a function of $z_{\rm re}$ for different values of Σm_ν. The colour coding is the same as in Fig. 3. The grey-shaded area encloses the central 34 light-cones (68 per cent of the total) for the N0 model only. The green diamond with error bars (1σ) and green-shaded area shows the results of $z_{\rm re} = 8.8^{+1.7}_{-1.4}$ and $\mathcal{D}_{3000}^{\rm kSZ} = (2.9 \pm 1.3)$ μK^2 by Planck Collaboration XIII (2016) and George et al. (2015), respectively. Bottom panel: relative differences with respect to the N0 model.

45 per cent, respectively, with respect to the ΛCDM model. This indicates that the effect of these two variables on the kSZ power spectrum can be studied independently. The plot of Fig. 5 also shows the combined results by Planck Collaboration XIII (2016) on $z_{\rm re}$, obtained with the assumption of instantaneous reionization, and on $\mathcal{D}_{3000}^{\rm kSZ}$ by George et al. (2015): as expected all models fit within 1σ, indicating that more precise measurements of the two observables need to be achieved to constrain Σm_ν.

In order to provide a more precise estimate of the dependence of $\mathcal{D}_\ell^{\rm kSZ}$ on $z_{\rm re}$ and neutrino mass, we fit our results on the kSZ power spectrum with the following relation:

$$\mathcal{D}_\ell^{\rm kSZ} = \mathcal{D}_{0,\ell}^{\rm kSZ}\, z_{\rm re}^{\alpha}\, (1 - f_\nu)^{\beta}\,, \qquad (11)$$

where $\mathcal{D}_{0,\ell}^{\rm kSZ}$ is the result for our fiducial model that assumes $f_\nu = 0$ (N0 run) and $z_{\rm re} = 8.8$. In Table 2, we show the best-fitting values (last two columns) of α and β computed separately for different values of ℓ, together with the $\mathcal{D}_\ell^{\rm kSZ}$ value of our N0 run and the same value after applying the box volume correction described in Section 4. The dependence on $z_{\rm re}$ is higher for low multipoles, going from $\alpha = 0.48$ at $\ell = 1000$ to $\alpha \simeq 0.2$ at $\ell > 5000$: this trend is justified by the shape of density/velocity perturbations at $z \simeq 9$ that peak slightly at 5–10 arcmin.

These results can be compared with the ones by Shaw et al. (2012), obtained with a completely different approach but similar cosmological parameters: they obtain a steeper dependence for both their non-radiative (NR) model, with values of 0.3–0.4, and cooling star formation (CSF), with values of 0.4–0.6. This difference with respect to their NR model appears to be connected to the treatment of low-redshift gas: in fact, their cumulative contribution of the kSZ effect (see their fig. 6) shows a fraction of about 50 per cent of kSZ effect associated with the redshift range of $0 < z < 2$, compared to our 61 per cent. This indicates that their method is underestimating the contribution in the non-linear regime (for a detailed explanation, see Park et al. 2016), thus reducing the kSZ at low redshift and steepening their relation at higher z. In their CSF run, this effect adds to the overcooling problem present in their simulation that

Table 2. Amplitude of the kSZ effect power spectrum, $\mathcal{D}_\ell^{\rm kSZ}$, and its dependence with $z_{\rm re}$ and Σm_ν. First column: multipole ℓ. Second column: value of $\mathcal{D}_\ell^{\rm kSZ}$, in $\mu{\rm K}^2$, obtained assuming $\Sigma m_\nu = 0$ (N0 run) computed averaging over the 50 light-cones (3.24 deg^2 each). Third column: $\mathcal{D}_\ell^{\rm kSZ}$ after applying a correction that accounts for a 20 per cent of missing signal due to the limited box size (see Section 4). The last two columns show the dependence of $\mathcal{D}_\ell^{\rm kSZ}$ on the redshift of reionization and neutrino mass fraction, computed as ${z_{\rm re}}^\alpha\,(1-f_\nu)^\beta$ (see equation 11).

ℓ	$\mathcal{D}_\ell^{\rm kSZ}$ $(\mu{\rm K}^2)$		${z_{\rm re}}^\alpha\,(1-f_\nu)^\beta$	
	Uncorr.	Vol. corr.	α	β
1000	1.88	2.4	0.48	12.4
2000	2.79	3.5	0.29	13.6
3000	3.21	4.0	0.26	14.3
4000	3.71	4.6	0.27	15.6
5000	3.74	4.7	0.24	14.2
6000	4.07	5.1	0.23	15.1
8000	4.21	5.3	0.18	15.0
10 000	4.32	5.4	0.20	15.1
15 000	4.39	5.5	0.17	16.1
20 000	4.19	5.2	0.15	16.4

they do not correct (see, instead, our correction with equation 7). This causes a further reduction of the low-redshift contribution.

The dependence on neutrino mass shows an opposite trend as a function of the multipole, increasing from $\beta = 14.3$ at $\ell = 3000$ to $\beta = 16.4$ at $\ell = 20000$. This is similar to the expected behaviour of the dependence with σ_8 (see Shaw et al. 2012), suggesting that even with a measurement of $\mathcal{D}_\ell^{\rm kSZ}$ at different multipoles it is difficult to break the Σm_ν–σ_8 degeneracy. However it is interesting to point out that the dependence with f_ν of the tSZ power spectrum is significantly different: Roncarelli et al. (2015) found that its normalization scales as $\mathcal{D}_\ell^{\rm tSZ} \propto (1-f_\nu)^{25-30}$, so approximately with a double steepness with respect to the kSZ equivalent at $\ell = 3000$. On the other hand, it is known that the dependence of the two power spectra with σ_8 shows less differences: in fact, the kSZ effect scales as $\mathcal{D}_\ell^{\rm kSZ} \propto {\sigma_8}^5$, while the tSZ effect only slightly steeper, with $\mathcal{D}_\ell^{\rm tSZ} \propto {\sigma_8}^{7-8}$ (Shaw et al. 2010, 2012; Trac et al. 2011; Horowitz & Seljak 2016). This suggests that a combined tSZ–kSZ observation can help break the degeneracy between the effect of massive neutrinos and σ_8. This point can be understood considering that, unlike the kSZ, the tSZ effect is dominated by small-scale perturbations of the IGM (i.e. galaxy clusters and groups). At large wave numbers, the suppression of the amplitude of the matter power spectrum induced by neutrinos is almost scale-independent, therefore, at that regime, the effects of massive neutrinos and variations of σ_8 are degenerate, and observables that are sensitive to these scales will exhibit that behaviour. A standard way to break this type of degeneracy consists in combining observables on small scales, such as the halo mass function of the Ly-α forest, with the ones more sensitive to large the ones like CMB, BAO or, as discussed here, kSZ effect power spectrum.

4 SYSTEMATIC EFFECTS

One of the main challenges in modelling the kSZ effect properties with simulations is the necessity of runs with both large volumes and high resolution: in fact, the kSZ effect is the result of the coupling between the large-scale velocity modes and the small-scale non-linear gas motions. In this section, we will use our second simulation set to investigate the possible systematics in our modelling of the kSZ power spectrum due to finite resolution and limited box size.

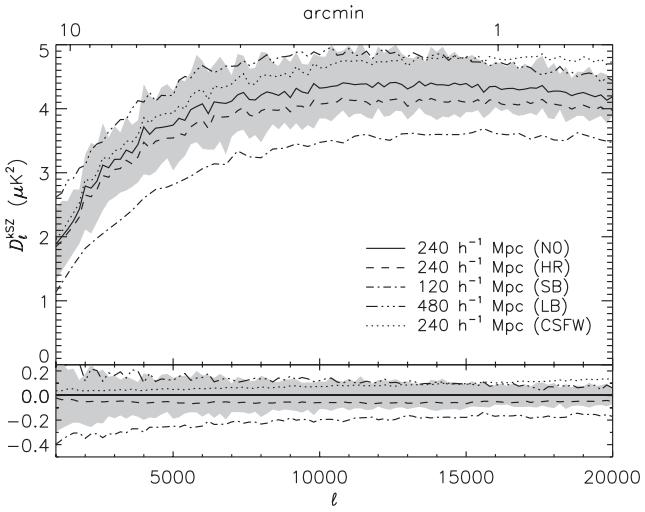

Figure 6. Same as Fig. 4 but for the second simulation set, i.e. assuming massless neutrinos with varying simulation parameters and physics. The solid line shows the average obtained from our reference model, N0, with the grey-shaded area that encloses the central 34 light-cones (68 per cent of the total). The dashed, dot–dashed, dot–dot–dot–dashed and dotted lines correspond to the average of the HR, SB, LB and CSFW simulations, respectively (see details in Table 1).

In addition, we will use our CSFW run to assess the reliability of our physical treatment of the IGM in describing the kSZ properties.

The plot in Fig. 6 shows the kSZ effect power spectrum as a function of the multipole ℓ assuming $z_{\rm re} = 8.8$ and massless neutrinos but varying simulation parameters. Since the N0 and HR simulations differ only for the mass resolution, a comparison between the two isolates the dependence on this parameter. The two power spectra are almost identical at low ℓ, while the amplitude of the HR simulation is lower by about 5 per cent for $\ell > 3000$. This small difference is due to the star fraction correction, described by equation (7): since the HR simulation predicts a significantly higher star formation (see Fig. 1) and since we apply the same correction on all the particles belonging to the same redshift and not in the exact position where star particles are formed, this perfectly accounts for the missing power of the HR simulation at large scales, but fails to recover the full signal at small ones. The fact that despite the extreme value of $f_\star(z)$ predicted by the HR model we are able to get almost the same result as for the N0 power spectrum, indicates that for more realistic star formation histories, like the ones of our first simulation set, our method is able to mimic the star formation history of Ilbert et al. (2013) without introducing significant systematics due to the lack of spatial information. This is partially confirmed by the analysis of the CSFW power spectrum, which shows a slightly higher amplitude with respect to the N0 one (less than 5 per cent for $\ell < 5000$). However, at higher multipoles the IGM feedback starts to play a non-negligible role, with galactic winds that increase the difference up to 10 per cent at $\ell \simeq 15000$ (see also the discussion in Roncarelli et al. 2007).

We test the impact of limited volume by using the results of the other two simulations, SB and LB, and comparing them with an analytical prediction. Iliev et al. (2007) defined a method to estimate the amount of missing velocity power based on the linear theory: we refer the reader to their work for the details of the procedure, and summarize the final result. When the power spectrum of the

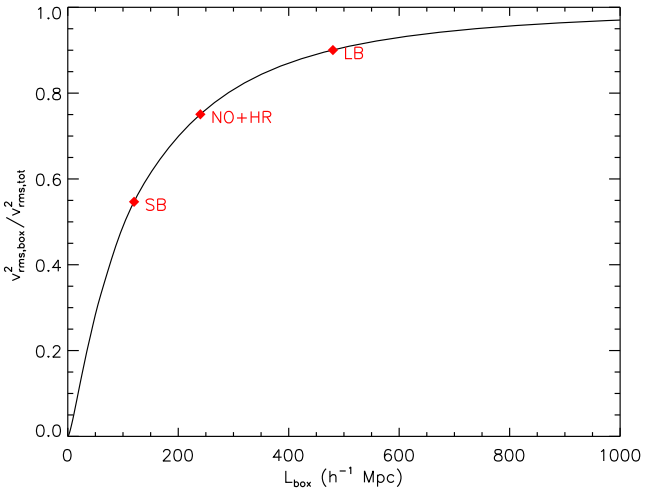

Figure 7. Fraction velocity power as a function of simulation box size in the linear-theory approximation. The red diamonds show the values of our second simulation set (see Table 1 for details).

velocity field, $P_{vv}(k)$, is known it is possible to calculate its rms in the following way:

$$v^2_{\rm rms} = \int_{k_{\rm min}}^{k_{\rm max}} \frac{k^2 P_{vv}(k)}{2\pi^2}\,{\rm d}k\,, \qquad (12)$$

where k is the wavenumber. Since $P_{vv}(k)$ decreases rapidly at small scales, the result depends on the value of $k_{\rm min} = 1/L_{\rm box}$ that can be adjusted according to the sampled volume. Therefore, we can compute the density power spectrum $P_{\delta\delta}(k)$ in the linear-theory approximation using CAMB with our reference ΛCDM cosmology,[5] then derive $P_{vv}(k)$ using the mass conservation equation and compute the value of $v^2_{\rm rms}$ as a function of the simulation box size. Fig. 7 shows the fraction of total linear-theory velocity power as a function of $L_{\rm box}$.

This method predicts that our N0 simulation misses the 25 per cent of the total linear velocity power, while about half and 10 per cent should be missed by the SB and LB runs, respectively. Obviously, the linear prediction serves only as an indication of possible biases since at the angular scales of interest for this work the kSZ effect receives a significant contribution from the low-redshift Universe (see Fig. 5), thus also by gas already in the non-linear regime whose dynamics should be well described by our hydrodynamical simulations. Analysing the results of Fig. 6, we do observe a significant damping for the SB with respect to the N0 run: about 20 per cent at large ℓ, with respect to about 30 per cent predicted by the linear theory. Most interestingly, the value of $\mathcal{D}^{\rm kSZ}_{3000}$ for the LB model is 3.73 μK^2, so the N0 result of 3.21 μK^2 is lower by 14 per cent, with respect to almost 20 per cent predicted by the linear theory. This indicates that although our $240\,h^{-1}$ Mpc box is lacking part of the large-scale velocity power, the linear-theory approximation slightly overestimates this amount. With the data that we have it is difficult to provide a precise value of the amount of kSZ signal that is missing due to the limited box size, and its dependence on the angular scale. However, given what said above, we estimate it to be about 20 per cent and add the volume corrected values of $\mathcal{D}^{\rm kSZ}_{\ell}$ in the third column of Table 2.

[5] We verified that the result on the missing power in the linear-theory approximation does not change significantly when introducing non-zero Σm_ν.

When accounting for this correction, we point out that our prediction on the kSZ power spectrum at $\ell = 3000$ for the ΛCDM model becomes $\mathcal{D}^{\rm kSZ}_{3000} = 4.0$ μK^2, thus significantly higher with respect to what obtained by several previous works, such as Battaglia et al. (2010), Trac et al. (2011) and Shaw et al. (2012), even if we are assuming a lower value of $z_{\rm re} = 8.8$ instead of the more popular $z_{\rm re} = 10$. Again, this is associated with the fact that previous simulations did not correct for the overcooling problem, hence overestimating the amount of star formation that, instead, we calibrate on observational data. On the other hand, the estimate of Shaw et al. (2012) is likely subject to an underestimate of the kSZ signal at low redshift (see the discussion in Section 3.2). An important consequence is that when applying this correction our constraints on patchy reionization become significantly tighter with respect to previous estimates. In detail, combining our result with the SPT measurement of $\mathcal{D}^{\rm kSZ}_{3000} = (2.9 \pm 1.3)$ μK^2 (George et al. 2015), we obtain an upper limit of $\mathcal{D}^{\rm kSZ,patchy}_{3000} < 1.0$ μK^2 (95 per cent CL).

5 SUMMARY AND CONCLUSIONS

In this paper, we have analysed a set of four cosmological hydrodynamical simulations to study how massive neutrinos influence the properties of the kSZ effect due to the IGM after reionization. Our runs have been carried out with the TREEPM+SPH code GADGET-III, following the evolution of three different particle types: gas, CDM and massive neutrinos in a box of $240\,h^{-1}$ Mpc per side. Starting from their outputs at different redshifts, we have produced 50 light-cone realizations from which we computed a set of Doppler b-parameter maps for each model, and relative kSZ power spectrum keeping track of the information in 20 redshift bins in the interval $0 < z < 15$. Since our simulations followed star formation with a simplified model, we corrected their output value of $f_\star(z)$ in order to match the current observational results (UltraVISTA data by Ilbert et al. 2013). In addition, we have done the same analysis on a set of four simulations with massless neutrinos but varying the resolution, box size and physical prescription, to study possible systematic effects.

Our results can be summarized as follows.

(i) In agreement with previous findings (Roncarelli et al. 2007), the typical values of the relative temperature variations are of the order of 10^{-6}, with peaks of 10^{-5}. For all models, the distribution of temperature fluctuations is well represented by a Gaussian curve, whose dispersion decreases with increasing neutrino mass as $\sigma_{b,\nu} = \sigma_{b,0}(1 - f_\nu)^{5.2}$.

(ii) The kSZ effect at large scales can be described with good precision (about 5 per cent at $\ell < 5000$) adopting simulations with simple physical prescription, by applying a correction that accounts for the uncertainty in the star mass fraction.

(iii) Using the second simulation set, we verified how our results depend on the limited box size, and verified that the linear-theory approximation slightly overestimates the amount of missing velocity power. Given our box size of $240\,h^{-1}$ Mpc per side we estimate that we are missing about 20 per cent of the total kSZ power spectrum, instead of the 25 per cent predicted by the linear theory.

(iv) In our ΛCDM model, we obtain a value of $\mathcal{D}^{\rm kSZ}_{3000} = 3.21$ μK^2, which becomes $\mathcal{D}^{\rm kSZ}_{3000} = 4.0$ μK^2 if we add the expected missing velocity power, enough to account for all of the SPT measurement of $\mathcal{D}^{\rm kSZ}_{3000} = (2.9 \pm 1.3)$ μK^2 (George et al. 2015). With currently favoured cosmological parameters, this points towards a rapid reionization scenario and translates into a stringent upper limit to the

possible kSZ effect contribution from patchy reionization models of $\mathcal{D}_{3000}^{\mathrm{kSZ,patchy}} < 1.0\ \mu\mathrm{K}^2$ (95 per cent CL).

(v) Massive neutrinos induce a reduction of the kSZ power spectrum at all angular scales of about 8, 12 and 40 per cent for $\Sigma m_\nu = (0.15, 0.3, 0.6)$ eV, respectively. All models agree within 1σ with the SPT measurement indicating that current kSZ data alone cannot provide interesting constraints on Σm_ν.

(vi) We studied how the value of the kSZ power spectrum scales with z_{re} and Σm_ν (see Table 2). At $\ell = 3000$, without fiducial values, we obtain $\mathcal{D}_{3000}^{\mathrm{kSZ}} \propto {z_{\mathrm{re}}}^{0.26}(1 - f_\nu)^{14.3}$. We observe that the dependence on $(1 - f_\nu)$ is significantly shallower with respect to the tSZ equivalent, that is expected to scale as $\mathcal{D}_\ell^{\mathrm{tSZ}} \propto (1 - f_\nu)^{25-30}$ (Roncarelli et al. 2015). Since the scaling of the two quantities with σ_8 is more similar (${\sigma_8}^5$ and ${\sigma_8}^{7-8}$ for the kSZ and tSZ effect, respectively), this suggests that a combined measurement of the two power spectra may represent an additional way to break the Σm_ν–σ_8 degeneracy.

Despite the relatively large error bars of the first kSZ power spectrum measurement (Crawford et al. 2014; George et al. 2015), our results show that this type of observable is extremely promising in providing information on the history of LSS formation. In fact, we have shown that with current ΛCDM cosmology the kSZ due to post-ionization already exceeds the nominal value and is close to the $+1\sigma$ limit, providing interesting constraints on several astrophysical and cosmological models. Indeed, besides patchy reionization, several non-standard cosmologies, like quintessence (Ratra & Peebles 1988; Wetterich 1988), modified gravity (see e.g. Hu & Sawicki 2007) and coupled dark energy (Wetterich 1995; Amendola 2000; Baldi 2011), generically predict an excess of velocity power spectrum with respect to standard ΛCDM (Jennings et al. 2012; Li et al. 2012; Ma & Zhao 2014; Bianchini & Silvestri 2016; Baldi & Villaescusa-Navarro 2016). On the other hand the presence of massive neutrinos, which represent a necessary ingredient for any realistic cosmological model, results in a reduction of the kSZ effect and must be taken into account before rejecting any of the mentioned model based on their predicted excess in the kSZ signal.

In this framework, further theoretical analyses are required, in particular simulations of larger cosmological volumes to account for the full velocity power spectrum and a more extended sampling of the parameter space for both standard (as e.g. Ω_{m} and σ_8) and non-standard (as e.g. dark energy and modified gravity) cosmological parameters aimed at studying possible intrinsic degeneracies. These detailed models, that we plan for our future works, will be necessary in the perspective to interpret current and possible future kSZ effect observations by, e.g. *Planck*, ALMA, ACT and ACTPol or the future generation of microwave telescopes.

ACKNOWLEDGEMENTS

This work has been supported by ASI (Italian Space Agency) through the Contract n. 2015-046-R.0. MR also acknowledges financial contribution from the agreement ASI n. I/023/12/0 '*Attività relative alla fase B2/C per la missione Euclid*'. The work of FVN is supported by the Simons Foundation. The work of FVN has been supported by the ERC-StG 'cosmoIGM' and partially supported by INFN IS PD51 'INDARK'. MB acknowledges support from the Italian Ministry for Education, University and Research (MIUR) through the SIR individual grant SIMCODE, project number RBSI14P4IH. We thank an anonymous referee that provided useful comments that improved the quality of our work. We also thank C. Carbone, S. Ettori, L. Moscardini, E. Vanzella, M. Viel and G. Zamorani for useful suggestions and discussions.

REFERENCES

Ahmad Q. R. et al., 2001, Phys. Rev. Lett., 87, 071301
Ahmad Q. R. et al., 2002, Phys. Rev. Lett., 89, 011301
Amendola L., 2000, Phys. Rev. D, 62, 043511
Baldi M., 2011, MNRAS, 411, 1077
Baldi M., Villaescusa-Navarro F., 2016, preprint (arXiv:1608.08057)
Baldi M., Villaescusa-Navarro F., Viel M., Puchwein E., Springel V., Moscardini L., 2014, MNRAS, 440, 75
Battaglia N., Bond J. R., Pfrommer C., Sievers J. L., Sijacki D., 2010, ApJ, 725, 91
Beutler F. et al., 2014, MNRAS, 444, 3501
Bianchini F., Silvestri A., 2016, Phys. Rev. D, 93, 064026
Carbone C., 2013, Nucl. Phys. B, 237, 50
Costanzi Alunno Cerbolini M., Sartoris B., Xia J.-Q., Biviano A., Borgani S., Viel M., 2013, J. Cosmol. Astropart. Phys., 6, 20
Crawford T. M. et al., 2014, ApJ, 784, 143
Croft R. A. C., Hu W., Davé R., 1999, Phys. Rev. Lett., 83, 1092
Cuesta A. J., Niro V., Verde L., 2016, Phys. Dark Universe, 13, 77
Elgarøy Ø. et al., 2002, Phys. Rev. Lett., 89, 061301
Fukuda Y. et al., 1998, Phys. Rev. Lett., 81, 1562
George E. M. et al., 2015, ApJ, 799, 177
Gonzalez-Garcia M., 2014, Phys. Dark Universe, 4, 1
Hand N. et al., 2012, Phys. Rev. Lett., 109, 041101
He J.-h., 2013, Phys. Rev. D, 88, 103523
Hinshaw et al., 2013, ApJS, 208, 19
Horowitz B., Seljak U., 2016, preprint (arXiv:1609.01850)
Hu W., Sawicki I., 2007, Phys. Rev. D, 76, 064004
Ilbert O. et al., 2013, A&A, 556, A55
Iliev I. T., Pen U.-L., Bond J. R., Mellema G., Shapiro P. R., 2007, ApJ, 660, 933
Iliev I. T., Mellema G., Pen U.-L., Bond J. R., Shapiro P. R., 2008, MNRAS, 384, 863
Iliev I. T., Mellema G., Ahn K., Shapiro P. R., Mao Y., Pen U.-L., 2014, MNRAS, 439, 725
Jennings E., Baugh C. M., Li B., Zhao G.-B., Koyama K., 2012, MNRAS, 425, 2128
Komatsu E. et al., 2009, ApJS, 180, 330
Komatsu E. et al., 2011, ApJS, 192, 18
La Vacca G., Kristiansen J. R., Colombo L. P. L., Mainini R., Bonometto S. A., 2009, J. Cosmol. Astropart. Phys., 0904, 007
Leistedt B., Peiris H. V., Verde L., 2014, Phys. Rev. Lett., 113, 041301
Lesgourgues J., Pastor S., 2006, Phys. Rep., 429, 307
Lesgourgues J., Pastor S., 2012, preprint (arXiv:1212.6154)
Lesgourgues J., Pastor S., 2014, New J. Phys., 16, 065002
Lesgourgues J., Mangano G., Miele G., Pastor S., 2013, Neutrino Cosmology. Cambridge Univ. Press, Cambridge
Lewis A., Challinor A., Lasenby A., 2000, ApJ, 538, 473
Li B., Hellwing W. A., Koyama K., Zhao G.-B., Jennings E., Baugh C. M., 2012, MNRAS, 428, 743
McQuinn M., Furlanetto S. R., Hernquist L., Zahn O., Zaldarriaga M., 2005, ApJ, 630, 643
Ma Y.-Z., Zhao G.-B., 2014, Phys. Lett. B, 735, 402
Mak D. S. Y., Pierpaoli E., 2013, Phys. Rev. D, 87, 103518
Mantz A., Allen S. W., Rapetti D., 2010, MNRAS, 406, 1805
Mantz A. B. et al., 2015, MNRAS, 446, 2205
Marulli F., Carbone C., Viel M., Moscardini L., Cimatti A., 2011, MNRAS, 418, 346
Mesinger A., McQuinn M., Spergel D. N., 2012, MNRAS, 422, 1403
Motohashi H., Starobinsky A. A., Yokoyama J., 2013, Phys. Rev. Lett., 110, 121302
Ostriker J. P., Vishniac E. T., 1986, ApJ, 306, L51
Palanque-Delabrouille N. et al., 2015, J. Cosmol. Astropart. Phys., 11, 011
Park H., Komatsu E., Shapiro P. R., Koda J., Mao Y., 2016, ApJ, 818, 37

Planck Collaboration XIII, 2016, A&A, 594, A13
Planck Collaboration XVI, 2014, A&A, 571, A16
Planck Collaboration XX, 2014, A&A, 571, A20
Planck Collaboration XXIV, 2016, A&A, 594, A24
Planck Collaboration XXXVII, 2016, A&A, 586, A140
Ratra B., Peebles P. J. E., 1988, Phys. Rev. D, 37, 3406
Roncarelli M., Moscardini L., Tozzi P., Borgani S., Cheng L. M., Diaferio A., Dolag K., Murante G., 2006, MNRAS, 368, 74
Roncarelli M., Moscardini L., Borgani S., Dolag K., 2007, MNRAS, 378, 1259
Roncarelli M., Moscardini L., Branchini E., Dolag K., Grossi M., Iannuzzi F., Matarrese S., 2010, MNRAS, 402, 923
Roncarelli M., Cappelluti N., Borgani S., Branchini E., Moscardini L., 2012, MNRAS, 424, 1012
Roncarelli M., Carbone C., Moscardini L., 2015, MNRAS, 447, 1761
Saito S., Takada M., Taruya A., 2011, Phys. Rev. D, 83, 043529
Sánchez A. G. et al., 2014, MNRAS, 440, 2692
Sayers J. et al., 2013, ApJ, 778, 52
Shaw L. D., Nagai D., Bhattacharya S., Lau E. T., 2010, ApJ, 725, 1452
Shaw L. D., Rudd D. H., Nagai D., 2012, ApJ, 756, 15
Shimon M., Rephaeli Y., Itzhaki N., Dvorkin I., Keating B. G., 2012, MNRAS, 427, 828
Springel V., 2005, MNRAS, 364, 1105
Springel V., Hernquist L., 2003, MNRAS, 339, 289
Sunyaev R. A., Zeldovich Y. B., 1970, Ap&SS, 7, 3
Tegmark M. et al., 2006, Phys. Rev. D, 74, 123507
Thomas S. A., Abdalla F. B., Lahav O., 2010, Phys. Rev. Lett., 105, 031301
Trac H., Bode P., Ostriker J. P., 2011, ApJ, 727, 94
Ursino E., Galeazzi M., Roncarelli M., 2010, ApJ, 721, 46
Viel M., Haehnelt M. G., Springel V., 2010, J. Cosmol. Astropart. Phys., 6, 15
Viel M., Becker G. D., Bolton J. S., Haehnelt M. G., 2013, Phys. Rev. D, 88, 043502
Villaescusa-Navarro F., Bull P., Viel M., 2015, ApJ, 814, 146
Vishniac E. T., 1987, ApJ, 322, 597
Wetterich C., 1988, Nucl. Phys. B, 302, 668
Wetterich C., 1995, A&A, 301, 321
Zahn O., Zaldarriaga M., Hernquist L., McQuinn M., 2005, ApJ, 630, 657
Zennaro M., Bel J., Villaescusa-Navarro F., Carbone C., Sefusatti E., Guzzo L., 2016, preprint (arXiv:1605.05283)
Zhao G.-B. et al., 2013, MNRAS, 436, 2038

This paper has been typeset from a TEX/LATEX file prepared by the author.